HHS Public Access

Author manuscript

Dev Biol. Author manuscript; available in PMC 2018 December 15.

Published in final edited form as:

Dev Biol. 2017 December 15; 432(2): 248–257. doi:10.1016/j.ydbio.2017.10.009.

Separate transcriptionally regulated pathways specify distinct classes of sister dendrites in a nociceptive neuron

Barbara M. J. O'Brien[a,b], **Sierra D. Palumbos**[a,c], **Michaela Novakovic**[a,d,1], **Xueying Shang**[a,e,2], **Lakshmi Sundararajan**[a,f], and **David M. Miller III**[a,g,*]

[a]3120 MRB III, Vanderbilt University, Nashville, TN 37240-7935

Abstract

The dendritic processes of nociceptive neurons transduce external signals into neurochemical cues that alert the organism to potentially damaging stimuli. The receptive field for each sensory neuron is defined by its dendritic arbor, but the mechanisms that shape dendritic architecture are incompletely understood. Using the model nociceptor, the PVD neuron in *C. elegans,* we determined that two types of PVD lateral branches project along the dorsal/ventral axis to generate the PVD dendritic arbor: (1) Pioneer dendrites that adhere to the epidermis, and (2) Commissural dendrites that fasciculate with circumferential motor neuron processes. Previous reports have shown that the LIM homeodomain transcription factor MEC-3 is required for all higher order PVD branching and that one of its targets, the claudin-like membrane protein HPO-30, preferentially promotes outgrowth of pioneer branches. Here, we show that another MEC-3 target, the conserved TFIIA-like zinc finger transcription factor EGL-46, adopts the alternative role of specifying commissural dendrites. The known EGL-46 binding partner, the TEAD transcription factor EGL-44, is also required for PVD commissural branch outgrowth. Double mutants of *hpo-30* and *egl-44* show strong enhancement of the lateral branching defect with decreased numbers of both pioneer and commissural dendrites. Thus, HPO-30/Claudin and EGL-46/EGL-44 function

*Corresponding author: David M. Miller, III PhD, Professor, Cell and Developmental Biology, PMB 407935, Rm 3120 MRB III, Vanderbilt University, Nashville, TN 37240-7935, (615) 343-3447, david.miller@vanderbilt.edu, https://medschool.vanderbilt.edu/miller-lab/.

[1]Present Address: Interdepartmental Neuroscience Graduate Program, Northwestern University, 320 East Superior St., Morton Building 1-645, Chicago, IL 60611-3010

[2]Present Address: Yale Combined Program in the Biological and Biomedical Sciences, Yale University, New Haven, CT 06520

[b]barbara.obrien@vanderbilt.edu

[c]s.palumbos@vanderbilt.edu

[d]michaelanovakovic@u.northwestern.edu

[e]xueyingshang@outlook.com

[f]lakshmi.sundararajan@vanderbilt.edu

[g]david.miller@vanderbilt.edu

Author contributions

DMM and BMJO designed the study; SDP performed the smFISH experiment; MN generated double mutants of *egl-46*/*egl-44* with *mec-3* for marker gene analysis and quantified 1° branch presence/absence; XYS quantified primary branch outgrowth defects in *mec-3* mutants; LS generated the PVD::mCherry::RAB-3 transgenic line; all other genetics, data collection, and analyses were performed by BMJO; DMM and BMJO wrote the manuscript with input from coauthors.

Conflicts of interest: none.

downstream of MEC-3 and in parallel acting pathways to direct outgrowth of two distinct classes of PVD dendritic branches.

Keywords

dendrite development; *C. elegans*; EGL-46; MEC-3; PVD; nociceptor

Introduction

Nociceptive neurons extend dendrites in the skin to detect noxious signals that evoke aversive responses to painful stimuli. Despite the importance of dendritic architecture to this function, the genetic pathways that specify nociceptor morphogenesis are incompletely understood.

We are using a model nociceptor, the bilateral PVD neuron in *C. elegans,* to investigate the mechanism of dendritic morphogenesis. Two PVD neurons, one on the left side of the body (PVDL) and the other on the right (PVDR), adopt elaborately branched dendritic arbors (Figure 1a–b) that evoke an escape response upon exposure to harsh mechanical force, extreme temperature or hyperosmolarity (Chatzigeorgiou et al., 2010; Li et al., 2011; Mohammadi et al., 2013; Smith et al., 2013; Way and Chalfie, 1989). With its ready accessibility to live cell imaging, PVD has proven to be especially useful for genetic strategies to identify key determinants of dendritic architecture (Dong et al., 2013; Oren-Suissa et al., 2010; Salzberg et al., 2013; Smith et al., 2013; 2010). Of particular note is the finding that the conserved LIM homeodomain transcription factor MEC-3 is required for all lateral branching. *mec-3* mutants show a striking morphological phenotype in which each PVD neuron extends 1° dendrites along the body axis but then fails to produce the lateral or 2° branches that give rise to the elaborate network of PVD dendrites that normally envelops the animal (Smith et al., 2013; 2010; Tsalik et al., 2003) (Figure 1c). To identify potential *mec-3* targets that mediate dendritic branching, we used a gene expression profiling strategy to detect *mec-3*-regulated transcripts in PVD. This approach determined that *mec-3* promotes expression of the claudin-like membrane protein HPO-30 that stabilizes lateral PVD dendritic branches (Smith et al., 2013). Here we report that an additional MEC-3 target, also revealed by this study (Smith et al., 2013), the TFIIA-like zinc finger transcription factor EGL-46, functions in parallel to HPO-30 to promote PVD lateral branching

EGL-46 and its binding partner, the TEA domain transcription enhancer factor EGL-44, function together in *C. elegans* to regulate cell cycle exit in neural progenitors (Feng et al., 2013; Wu et al., 2001) and to define cell-specific traits in postmitotic neurons (Desai et al., 1988; Rojo Romanos et al., 2015; Wu et al., 2001; Yu et al., 2003). Our work previously revealed an additional role for EGL-46 in dendritic branching: *egl-46* mutant PVD neurons show fewer lateral branches than wild type (Smith et al., 2013; 2010; 2012). That the PVD lateral branching phenotype of *egl-46* is less severe than that of *mec-3* is consistent with our microarray results showing that EGL-46 is regulated by MEC-3 and the conclusion that MEC-3 likely controls more than one downstream effector of dendritic branching (Smith et

al., 2013). Here we substantiate this prediction by showing that HPO-30 and EGL-46 act in separate pathways to drive lateral branching and that these roles are correlated with two distinct classes of PVD dendrites. Approximately half of PVD lateral branches fasciculate with pre-existing circumferential motor neuron commissures that bridge the gap between dorsal and ventral nerve cords. In contrast to these "commissural" PVD branches, "pioneer" secondary branches grow out in contact with the epidermis but are not bundled with motor neuron commissures. We have previously shown that HPO-30 is preferentially required for stabilizing pioneer branches (Smith et al., 2013; 2010). Here we report that the EGL-44/EGL-46 complex exerts the complementary role of supporting commissural branch outgrowth. These findings point to a distinct class of downstream effectors of EGL-44/EGL-46 for either commissural branch formation or maintenance. Moreover, the finding that the 2° branching defect of double mutants of *egl-44* and *hpo-30* is less severe than that of *mec-3* argues for at least one additional lateral branch promoting pathway that is also regulated by MEC-3. Finally, our observation that *mec-3* also defines the overall lengths of the PVD axon and 1° dendrites, traits that are not regulated by *egl-44*/*egl-46*, is indicative of a separate class of *mec-3*-regulated targets that contribute to PVD morphogenesis. This work is important because it has revealed an intricate genetic program for specifying distinct morphological features of a model nociceptive neuron.

Material and Methods

Genetic Strains

All *C. elegans* strains were grown on OP50-1 *Escherichia coli*-seeded nematode growth medium plates at 20°C as described (Brenner, 1974). The N2 strain was used as the wild-type reference. Other strains used in this study are listed in Supplemental Table 1.

Molecular cloning and generation of transgenic animals

To generate the *PVD::EGL-46* plasmid pBMJO12, the *egl-46* coding region was amplified from N2 genomic DNA by the polymerase chain reaction (PCR) using 5′ and 3′ primers with adaptors for Asc1 (tttttGGCGCGCCATGGTGCCTATGAATGACTT) and SacII (acacaCCGCGGctagattcactttcagcaaa), respectively. The resultant fragment was digested with Asc1 and SacII and cloned into an expression plasmid (pBMJO1) containing the *F49H12.4* promoter. pBMJO12 (15 ng/ul) was co-injected with a PVD marker plasmid, pCJS04 (*F49H12.4:*:mCherry) (30 ng/ul) into the strain NC1686, which contains an integrated marker for PVD labeled with GFP (C. J. Smith, 2012). The resultant extrachromosomal array (*wdEx1006*) was then crossed into different genetic backgrounds by monitoring the *F49H12.4*::mCherry co-injection marker.

Plasmid pCJS06 (*F49H12.4*::mCherry::RAB-3) was injected into N2 at 10 ng/μl with the co-injection marker *Pmyo2*::mCherry (2 ng/ul). The resultant extrachromosomal array (*wdEx1005*) was then crossed into the *mec-3* mutant background by monitoring *Pmyo2*::mCherry.

Plasmid sequences are available upon request.

Single Molecules mRNA Fluorescence In Situ Hybridization (smFISH)

smFISH was performed with custom *egl-46* probes linked to CAL Fluor® Red 590 (Biosearch Technologies). Synchronized late L2-stage larvae were collected by washing plates with M9, fixed in 4% paraformaldehyde in 1X PBS for 45 minutes and permeabilized in 70% ethanol for 48 hours. Hybridization was performed as previously described (Smith et al., 2013). PVD was marked with *PVD::GFP* and cell nuclei stained with DAPI. Z-stacks were collected in a Nikon spinning disk confocal microscope with optical filters for DAPI, CAL Fluor® Red 590 and GFP using a 60X objective (NA = 1.4) in 0.5 um steps spanning the cell body and merged for quantification of smFISH puncta that exceeded a threshold set by CAL Fluor® Red 590 background signal and that were located within the GFP-labeled PVD cell body. smFISH staining was noted in separate *egl-46*-positive head neurons for all samples to confirm successful hybridization.

Quantification of neuronal features

Worms were immobilized with 15mM levamisole/0.05 tricaine on a 2% agarose pad in M9 (Smith et al., 2010). All images and quantitative data were obtained from L4 stage hermaphrodites. For quantification of 2° branches and 1° branch and axon length, confocal images were obtained on either a Leica TCS SP5 or Nikon A1R laser-scanning confocal microscope. Z-stacks were collected in 1 μm steps at 40X (oil objective, NA=1.3) to capture the cell body and all dendritic branches of each PVD neuron. Individual Z-stacks were merged into a single z projection to visualize 1° and 2° branches. A 2° branch was defined as a lateral branch that grew orthogonally from the 1° branch and reached the sublateral nerve cord. 2° branches that fasciculated with motor neuron commissures were counted as "commissural" branches, whereas 2° branches that did not fasciculate with motor neuron commissures were counted as "pioneer" branches. 1° branch length, axon length, and body length were measured using ImageJ. Branch or axon lengths were then divided by body lengths to obtain the branch/body or axon/body length ratios. PVD neurons were visualized with cytosolic GFP driven by the *F49H12.4* or *ser2prom3* promoters; motor neuron commissures were visualized with mCherry driven by the pan-neural marker *Prab-3*. For all experiments, the experimenter was blinded to condition when scoring. To score the presence or absence of the PVD posterior 1° branch, worms were examined with a Zeiss Axiovert microscope (40X oil objective, NA=1.3) and results pooled from three separate experiments.

Image collection for figures

Images were obtained at 40X (oil objective, NA=1.3, 1 μm steps) or 100X (oil objective, NA=1.49, 0.5 μm steps) on either a Leica TCS SP5 or Nikon A1R laser-scanning confocal microscope. Individual Z-stacks were merged into a single z-projection. All images shown throughout the figures are adjusted for brightness and contrast (ImageJ) for clarity and to decrease background autofluorescence but are otherwise unaltered.

Statistics

One-way ANOVA with Tukey's test for multiple comparisons was used for comparisons across multiple conditions. For posterior 1° branch presence/absence analysis, a contingency table was constructed for Fisher's Exact test. A Mann-Whitney test was used to determine

significance between the averages of the two groups for the smFISH experiment. For all other comparisons of averages between only two conditions, an unpaired t-test was used. Statistics were performed using Graphpad Prism 6.

Results

MEC-3 and EGL-46 promote outgrowth of lateral dendritic branches

We used the marker *PVD::GFP* to visualize PVD morphology (see Methods). In the wild type, each PVD neuron adopts a striking orthogonal array of dendritic branches; lateral 2° dendrites arise from a central 1° process to constitute the "trunk" of menorah-like structures festooned with 3° and 4° branches (Figure 1a–b) (Albeg et al., 2011; Oren-Suissa et al., 2010; Smith et al., 2010). We confirmed previous findings that both *mec-3* and *egl-46* are required for the full complement of PVD menorahs (Smith et al., 2013; 2010; Tsalik et al., 2003). In *mec-3* mutants, all lateral branches (2°, 3°, and 4°) are missing with only anterior and posterior 1° dendrites projecting along the body axis and a single axon extending from the PVD cell body into the ventral nerve cord (Figure 1c). The branching defect is less severe for *egl-46* mutants, which display approximately 25% fewer 2° branches than wild type (Supplemental Figure 1d). Throughout this work, 2° branches are defined as lateral PVD dendrites that extend the full distance from the 1° dendrite to the sublateral nerve cord (see Methods). Higher order 3° and 4° branches are apparently normal in *egl-46* mutants. The PVD 2° branch defects for *mec-3* and *egl-46* are highly significant ($p<0.0001$, each compared to wild type, one-way ANOVA with Tukey's test for multiple comparison, $n\geq20$) (Figure 1e). Similar results were obtained with the PVD-specific marker *ser2prom3::GFP* (Supplemental Figure 1).

EGL-44 and EGL-46 act in a common genetic pathway to regulate PVD 2° branching

Because other studies have shown that the TEA domain transcription factor EGL-44 typically functions in concert with EGL-46 to specify cell-specific traits in *C. elegans* (Rojo Romanos et al., 2015; Wu et al., 2001; Yu et al., 2003), we tested an *egl-44* mutant for PVD defects. This experiment revealed that the 2° branching defect of *egl-44* is virtually identical to that of *egl-46* ($p>0.05$, one-way ANOVA with Tukey's multiple comparison test) and also results in a modest but significant reduction (~25%) in PVD 2° branches ($p<0.001$ vs wt, one-way ANOVA with Tukey's multiple comparison test) (Figure 1e and Supplemental Figure 1e).

Given our finding that *egl-44* and *egl-46* mutants show similar deficits in the number of 2° branches, we generated an *egl-44;egl-46* double mutant to ask if *egl-44* and *egl-46* act in the same or different genetic pathways. *egl-44;egl-46* animals showed fewer 2° branches than wild type ($p<0.001$, one-way ANOVA with Tukey's multiple comparison test, $n\geq20$), but this feature did not differ significantly from that of either *egl-44* or *egl-46* single mutants ($p>0.05$, one-way ANOVA with Tukey's multiple comparison test, $n\geq20$) (Figure 1e). This result confirms the idea that *egl-44* and *egl-46* act in a common genetic pathway to mediate PVD 2° branching.

Expression of EGL-46 in PVD is sufficient to restore wild-type 2° branch number in egl-46 mutants

We have previously used microarray profiling to show that *egl-46* expression in PVD depends on *mec-3* (Smith et al., 2013). This result suggests that *egl-46* likely functions in PVD to promote 2° branch outgrowth. To test this idea, we fused the EGL-46 coding region to the PVD-specific *F49H12.4* promoter and determined that expression of the resultant PVD::EGL-46 transgene was sufficient to rescue the 2° branch defect of *egl-46* mutants ($p<0.0001$ for *egl-46* compared to *egl-46; PVD::EGL-46* and $p>0.05$ for *wt* compared to *egl-46;PVD::EGL-46*, one-way ANOVA with Tukey's multiple comparisons, $n\geq20$) (Figure 1e). Additionally, PVD expression of EGL-46 did not rescue *egl-44* ($p>0.05$ for *egl-44* compared to *egl-44;PVD::EGL-46*, one-way ANOVA with Tukey's test for multiple comparisons, $n\geq20$) (Figure 1e). These results are consistent with a cell autonomous role for EGL-46 in PVD lateral branching and the conclusion that this function depends on *egl-44*. Our finding that PVD::EGL-46 did not restore 2° branches to a *mec-3* mutant suggests that EGL-46-dependent branching also requires other factors that are independently regulated by *mec-3* ($p>0.05$ for *mec-3* compared to *mec-3;PVD::EGL-46,* one-way ANOVA with Tukey's test for multiple comparisons, $n\geq18$). Although this result could be explained by a model in which EGL-44 is down-regulated in the *mec-3* mutant, this possibility seems unlikely because our previous microarray results did not detect differences in *egl-44* transcript levels in the *mec-3* mutant PVD neuron (Smith et al., 2013). Thus, other MEC-3 targets are likely to function in parallel to the EGL-46/EGL-44-regulated pathway to generate 2° branches. Finally, the observation that PVD::EGL-46 does not induce additional 2° branches in the wild type ($p>0.05$ for *wt* compared to *wt;PVD::EGL-46*, one-way ANOVA with Tukey's multiple comparisons, $n\geq20$) suggests that EGL-46-dependent branching may also be limited by additional pathways that prevent the creation of ectopic 2° branches.

EGL-44/EGL-46 selectively promote the formation of commissural 2° branches

Having established that *egl-44* and *egl-46* mutants result in the elimination of only a fraction (~25%) of PVD lateral branches, we next considered the possibility that the *egl-44/egl-46* regulated pathway is required for a specific subset of 2° dendrites. In the first instance, we reanalyzed data from Figure 1e to rule out the possibility that *egl-44/egl-46* mutants selectively eliminate either dorsally or ventrally projecting 2° branches. A similar analysis did not detect any differences in *egl-44/egl-46* vs wild type between 2° branches that arise either anterior or posterior to the PVD cell soma (Supplemental Figure 2). Finally, we considered 2° branches that arise from PVDR on the right side of the animal vs PVDL on the left. We confirmed our previous finding (Smith et al., 2013) that PVDR contains more 2° branches than PVDL in the wild type ($p<0.001$, unpaired t-test, $n\geq7$) (Figure 2a, Supplemental Figure 3). This right-left bias was either reduced or absent in *egl-44* and *egl-46* mutants (Figure 2a, Supplemental Figure 3), despite a significant loss of 2° branches for both PVDR and PVDL. This finding is suggestive of a specific role for *egl-44*/*egl-46* in PVDR branching and provided an important clue to the subtype of 2° branch that depends on the *egl-44/egl-46* pathway.

We previously noted that a subset of PVD 2° branches fasciculate with commissures from ventral cord motor neurons and suggested that this interaction could stabilize the circumferential outgrowth of these "commissural" 2° branches. This idea is consistent with the observation that the majority of motor neuron commissures are located on the right side (Supplemental Figure 4a–b), that PVDR contains more 2° branches than PVDL, and that this right-left bias is abrogated by a genetic mutation that selectively eliminates motor neuron commissural outgrowth (Smith et al., 2013; 2010). We therefore hypothesized that the diminution of right-left bias in *egl-44* and *egl-46* mutants was due to the preferential loss of commissural branches. We tested this idea by determining the fraction of branches that fasciculate with motor neuron commissures (commissural branches) vs 2° branches that do not fasciculate with motor neuron commissures (pioneer branches) in PVDR (Figure 2b). In the wild type, PVDR shows a higher fraction (~60%) of commissural than pioneer branches (~40%) ($p<0.001$, unpaired t-test, n=20). This bias was not apparent, however, in mutants of *egl-44* ($p>0.05$, unpaired t-test, n=18) or *egl-46* ($p>0.05$, unpaired t-test, n=20) (Figure 2c) and cannot be attributed to reduced numbers of motor neuron commissural processes, which are normal in *egl-44* and *egl-46* mutants (Supplemental Figure 4c). Next, we counted the total number of PVDR commissural and pioneer branches and determined that commissural 2° branches are reduced in mutants of *egl-44* and *egl-46* compared to *wt* ($p<0.0001$, one-way ANOVA with Tukey's test for multiple comparison, $n\geq18$) but detected no significant differences for the number of PVDR pioneer branches across genotypes ($p>0.05$, one-way ANOVA with Tukey's test for multiple comparisons, $n\geq18$) (Figure 2d). These results suggest that the EGL-44/EGL-46 pathway specifically regulates downstream components involved in 2° branches that fasciculate with motor neuron commissures but is not required for pioneer branch outgrowth.

EGL-44 and HPO-30/Claudin act in complementary pathways to mediate 2° branch number

We recently determined that MEC-3 activates expression of the claudin-like membrane protein HPO-30 in PVDR neurons to mediate pioneer branch outgrowth; *hpo-30* mutants show a biased reduction in pioneer vs commissural PVDR 2° branches (Smith et al., 2013). Because *egl-44* and *egl-46* mutants display the opposite effect (i.e., biased loss of commissural vs pioneer branches), we hypothesized that *egl-44/egl-46* and *hpo-30* function in complementary pathways to regulate 2° branch outgrowth. To test this idea, we constructed double mutants of *egl-44* and *hpo-30* (Figure 3a–c, Supplemental Figure 5) and determined that *egl-44;hpo-30* animals showed significantly fewer 2° branches in PVDR than either single mutant ($p>0.05$ for *hpo-30* vs. *egl-44*, $p<0.05$ for *hpo-30* vs. *egl-44;hpo-30*, $p<0.01$ for *egl-44* vs. *egl-44;hpo-30*, one-way ANOVA with Tukey's test for multiple comparisons, $n\geq18$) (Figure 3e). This result is consistent with the model in which *egl-44* and *hpo-30* act in separate pathways.

If EGL-44 selectively promotes commissural branch outgrowth while HPO-30 favors pioneer branches as we have proposed, then PVDR in double mutants of *egl-44;hpo-30* should also show fewer commissural branches than *hpo-30* but not *egl-44*. We substantiated this prediction by quantifying commissural branches for these three mutant backgrounds ($p>0.05$ for *egl-44* vs. *egl-44;hpo-30*, $p<0.05$ for *hpo-30* vs. *egl-44;hpo-30*, $p<0.01$ for *hpo-30* vs. *egl-44*, one-way ANOVA with Tukey's test for multiple comparisons, $n\geq18$)

(Figure 3f). A similar analysis confirmed the additional expectation that PVDR in double mutants of *egl-44;hpo-30* should show fewer pioneer branches than *egl-44* but not *hpo-30* ($p>0.05$ for *hpo-30* vs. *egl-44;hpo-30*, $p<0.001$ for *hpo-30* vs. *egl-44*, $p<0.0001$ for *egl-44* vs. *egl-44;hpo-30*, one-way ANOVA with Tukey's test for multiple comparisons, $n\geq18$) (Figure 3g). Parallel studies of *egl-46/egl-44* function in PVDL were not performed due to the limited number of commissural 2° branches but it seems likely that PVDL dendrite morphogenesis is similarly regulated (Figure 2a).

These results suggest that commissural and pioneer PVD 2° branches are defined by separate genetic pathways. However, the significant number of residual 2° branches (roughly 50% of wild-type) in double mutants of *egl-44;hpo-30* and the absence of all 2° branches in a *mec-3* mutant suggest that MEC-3 likely regulates at least one additional pathway that promotes 2° branch outgrowth (Figure 3d).

MEC-3 determines 1° branch and axon length

Because the *mec-3* phenotype points to a critical role for MEC-3 in PVD lateral branching, we also considered the possibility of significant effects on other features of PVD architecture. In the wild type, the anterior 1° branch extends from the PVD soma to the base of the pharynx and the posterior 1° branch projects from the soma to the anus. We measured the lengths of anterior and posterior 1° branches (Figure 4a) and found that both the anterior and posterior branches were shorter in comparison to body length in mutants of *mec-3* ($p<0.0001$ vs wt, one-way ANOVA with Tukey's test for multiple comparisons, $n\geq20$) but not in mutants of *egl-44*, *egl-46*, or *egl-44;egl-46* ($p>0.05$, each compared to *wt*, one-way ANOVA with Tukey's test for multiple comparisons, $n\geq20$) (Figure 4b–c and Supplemental Figure 6a–d). Differences in 1° branch length could not be attributed to a change in the position of the PVD cell soma, as the ratio of the distance from PVD soma to the anus versus the distance of the PVD cell soma to the pharynx was not different in *mec-3* in comparison to wild-type ($p>0.05$, unpaired t-test, $n\geq20$) (Supplemental Figure 6e). A difference in 1° branch length was particularly noticeable in a fraction of *mec-3* mutants in which the posterior 1° branch was completely absent ($p<0.001$, *mec-3* vs. *wt*, Fisher's exact test, $n\geq40$) (Figure 4d, Supplemental Figure 6f), whereas *egl-44*, *egl-46*, and *egl-44;egl-46* mutants never showed this defect (data not shown).

We noted that *mec-3* mutants also affect the length of the PVD axon. Normally, the PVD axon adopts an L-shaped trajectory with a short ventral segment that turns as it enters the ventral nerve cord to project anteriorly (White et al., 1986). This overall morphology is preserved in *mec-3* mutants which do not show visible PVD axon guidance defects (data not shown) but do display a significantly longer axonal projection in the ventral nerve cord. PVD axonal length was not perturbed in *egl-46* mutants, however ($p<0.0001$ for *wt* vs. *mec-3* and for *egl-46* vs. *mec-3*, $p>0.05$ for *wt* vs. *egl-46*, one-way ANOVA with Tukey's test for multiple comparisons, $n\geq17$) (Figure 4e). Finally, we confirmed that the presynaptic vesicle-associated protein, mCherry::RAB-3, is localized throughout the length of the *mec-3* mutant axon as in the wild type, which therefore suggests that *mec-3* is not required for trafficking or localization of the presynaptic apparatus (Figure 4f).

MEC-3 and EGL-44/EGL-46 share redundant roles in regulating PVD-specific genes

Our results are consistent with a model in which *egl-46* expression is regulated by *mec-3* to control a group of downstream effector genes that promote commissural branch outgrowth. Additional results suggest, however, that a subset of PVD genes may be co-regulated by *mec-3* and by *egl-44*/*egl-46*. The reporter genes *ser2prom3::GFP* and *F49H12.4::GFP* are highly expressed in PVD in wild type, and PVD expression is maintained in single mutants of either *mec-3*, *egl-44*, or *egl-46*, and in double mutants of *egl-44;egl-46*. PVD expression of *ser2prom3::GFP* and *F49H12.4::GFP* is not detectable, however, in double mutants of either *egl-44;mec-3* or *egl-46;mec-3* but is readily visible in the adjacent PDE neuron (Figure 5, Supplemental Figure 7). To confirm that the PVD neuron is generated in *egl-44;mec-3* and *egl-46;mec-3* mutants, we used the pan-neural marker *Prab-3::mCherry* to label all neurons. In these animals, a single mCherry-labeled cell body is clearly visible directly anterior to PDE in the location usually occupied by PVD (Figure 5). These results suggest that *mec-3* and *egl-44*/*egl-46* may act independently to co-regulate a cohort "PVD-specific" genes.

Our previous microarray results detected *egl-46* as a *mec-3*-regulated transcript(Smith et al., 2013). The additional observation reported here that an *egl-46* mutant alters gene expression in a *mec-3* mutant background (e.g., loss of *ser2prom3::GFP*) argues for at least a residual level of EGL-46 expression in *mec-3* mutant PVD neurons. To test this idea, we used smFISH to quantify *egl-46* transcripts in PVD. This experiment confirmed that *egl-46* mRNA is significantly reduced in a *mec-3* mutant in comparison to wild type (Figure 6a, b) ($p<001$, Mann-Whitney test, $n>20$) (Figure 6c). *egl-46* mRNA puncta were still clearly visible in the *mec-3* mutant PVD neuron, however (Figure 6b, c). Thus, taken together, results shown Figure 5 and Figure 6 suggest that *egl-46* is regulated *mec-3* and by at least one additional upstream transcription factor to control PVD-specific traits (Figure 6d).

Discussion

The unique architectural features that define separate classes of neurons depend on the execution of specific genetic programs that drive morphogenesis. The importance of this developmental axis is underscored by the striking neuron-specific defects that are commonly observed for mutations that disable individual transcription factors (Grueber et al., 2003; Jinushi-Nakao et al., 2007; Moore et al., 2002; Parrish et al., 2006; Smith et al., 2013). Thus, the goal of elucidating the molecular pathways that govern neuron morphology requires the discovery of the downstream effectors of transcriptional activity. In our strategy to achieve this objective, we are utilizing an experimental approach in *C. elegans* that exploits the ready accessibility of the PVD nociceptive neuron for molecular genetic analysis and its stereotypical morphology for live cell imaging (Smith et al., 2013; 2012; 2010).

Each of the bilateral PVD neurons, arrayed on the left (PVDL) and right (PVDR) sides of the animal, displays the striking morphological features of a highly branched but well-ordered dendritic arbor placed directly beneath the skin and a single, unbranched axon that enters the ventral nerve cord to synapse with specific motor circuit targets (Albeg et al., 2011; Oren-Suissa et al., 2010; Smith et al., 2010; White et al., 1986). PVD functions as a polymodal nociceptor to trigger an escape response to the aversive stimuli of harsh

mechanical force, temperature extremes and hyperosmolarity (Chatzigeorgiou et al., 2010; Li et al., 2011; Mohammadi et al., 2013; Smith et al., 2013; Way and Chalfie, 1989). PVD dendritic morphology is defined by a repetitive motif of laterally projecting menorah-like structures that emanate from the axial 1° dendrites and terminate with a filigreed array of 4° branches (Figure 1) (Hall and Treinin, 2011). This characteristic dendritic morphology is radically simplified by mutations that inactivate the MEC-3 LIM homeodomain transcription factor. In *mec-3* mutants, lateral branching fails and dendritic menorahs are largely absent (Tsalik et al., 2003). We showed that *mec-3* function is required in PVD for the initiation of dendritic branching and used a cell-specific profiling strategy to identify *mec-3*-regulated genes (Smith et al., 2013; 2010). This approach determined that the claudin-like membrane protein HPO-30 functions downstream of *mec-3* to stabilize the 2° branches that normally give rise to each menorah. The biased effect of *hpo-30* mutants on pioneer 2° branches suggested that a different *mec-3*-regulated gene must be required for commissural 2° dendrites. We surmised that this component could be the MEC-3 target and TFIIA-like zinc finger transcription factor EGL-46, since lateral branches are also reduced in number but not completely eliminated in *egl-46* mutants (Smith et al., 2013; 2012; 2010). Here we have confirmed this prediction by showing that commissural branches are preferentially dependent on EGL-46 and its transcription factor binding partner EGL-44 (Figure 2d). Thus, parallel acting pathways involving either *hpo-30* or *egl-44*/*egl-46* are needed for the full complement of PVD menorahs (Figure 3d).

The branching function of HPO-30 depends on its expression in PVD. The LRR (Leucine Rich Repeat) protein DMA-1 likely acts in the same pathway as it shows a similar mutant PVD branching defect (Dong et al., 2013; Smith et al., 2013). DMA-1 mediates dendritic outgrowth as a PVD-expressed component of a quarternary complex containing the cell surface proteins SAX-7/L1CAM and Menorin/MNR-1 in the epidermis and the soluble factor LECT-2 (Díaz-Balzac et al., 2016; Dong et al., 2013; Liang et al., 2015; O'Brien et al., 2016; Salzberg et al., 2013; Zou et al., 2016). These interactions are necessary for 3° and 4° branching, but additional epidermal cues are likely required for pioneer 2° branch outgrowth as the *dma-1* mutant phenotype is more severe than that of either *sax-7*, *mnr-1*, or *lect-2*. Although *hpo-30* and *dma-1* preferentially affect pioneer branches, higher order branching for all menorahs is also disrupted. In contrast, menorahs containing pioneer 2° branches are apparently intact in *egl-44* and *egl-46* mutants. Thus, our results suggest that EGL-44/EGL-46 regulate downstream effectors that act selectively in commissural dendrites whereas HPO-30 and DMA-1 are needed for 3° and 4° branching in both classes of menorahs, in addition to their role in directing pioneer 2° dendrites. EGL-44/EGL-46 targets likely include downstream effectors that mediate fasciculation of PVD 2° dendrites with motor neuron commissures. Multiple cell surface proteins including Dscam (Bruce et al., 2017), members of the L1CAM family and receptor tyrosine kinases and phosphatases (Feng et al., 2013; Van Vactor, 1998; Wu et al., 2001) as well as secreted Ig domain proteins (Aurelio et al., 2002) have been shown to mediate inter-axonal fasciculation, but much less is known of the factors that direct dendritic bundling (Barry et al., 2010). Our observation that the *mec-3* PVD branching defect is more severe than that of double mutants in which both *hpo-30* and *egl-44* are inactivated suggests that dendrite morphogenesis also depends on other *mec-3*-regulated components. In addition, MEC-3 independently controls the length

of the PVD 1° dendrite and axon (Figure 4). Our ongoing studies of *mec-3*-regulated targets are designed to detect these genes (Smith et al., 2013). Finally, our results have also identified at least two PVD-expressed markers that are redundantly regulated by both MEC-3 and the EGL-44/EGL-46 complex (Figure 5). These observations point to a potentially complex transcriptional regulatory mechanism in which MEC-3 directs assembly of key architectural components of the PVD neuron by activating expression of *egl-46* and *hpo-30* and also functions in concert with EGL-44/EGL-46 to control a different subset of PVD-specific traits. Experiments with additional PVD-specific markers are needed to validate this hypothesis. The strong conservation of MEC-3-related LIM homeodomain proteins and of EGL-44 and EGL-46 in vertebrate genomes argues that similar transcriptional networks may regulate neuronal morphogenesis in the brain (Anbanandam et al., 2006; Desai et al., 1988; Feng et al., 2013; Hunter and Rhodes, 2005; Rojo Romanos et al., 2015; Rosenbaum et al., 2011).

Conclusions

This study utilized the PVD nociceptive neuron in *C. elegans* to determine that the TFIIA-like zinc finger transcription factor, EGL-46, and its binding partner, the TEAD transcription factor EGL-44, are required for PVD dendrites that fasciculate with pre-existing motor neuron commissures. This role complements a previously identified mechanism involving the claudin-like protein HPO-30 that selectively promotes outgrowth of pioneer PVD dendrites that do not fasciculate with motor neuron commissures. Both parallel-acting pathways function downstream of the LIM-homeodomain transcription factor MEC-3, which is required for all lateral PVD dendrites. Thus, our findings have revealed discrete transcriptionally-regulated pathways that specify separate classes of sister dendrites emanating from a single type of sensory neuron.

Supplementary Material

Refer to Web version on PubMed Central for supplementary material.

Acknowledgments

We thank C. J. Smith (University of Notre Dame) for generating the PVD::mCherry::RAB-3 plasmid, K. Shen (Stanford University) for *wyIs378*, O. Hobert (Columbia University) for *otIs181* and B. A. Millis in the Nikon Center of Excellence at Vanderbilt University for help with imaging smFISH results. Additional strains were provided by the *Caenorhabditis* Genetics Center (CGC), which is funded by NIH Office of Research Infrastructure Programs (P40 OD010440). This work was supported by NIH grant R01NS079611 to DMM, NSF grant DGE: 1445197 to SDP, a Vanderbilt Undergraduate Summer Research Program grant to MN, and a National Top Talent Undergraduate Program (NTTUTP) Fudan University grant to XYS.

References

Albeg A, Smith CJ, Chatzigeorgiou M, Feitelson DG, Hall DH, Schafer WR, Miller DM III, Treinin M. C. elegans multi-dendritic sensory neurons: morphology and function. Mol Cell Neurosci. 2011; 46:308–317. DOI: 10.1016/j.mcn.2010.10.001 [PubMed: 20971193]

Anbanandam A, Albarado DC, Nguyen CT, Halder G, Gao X, Veeraraghavan S. Insights into transcription enhancer factor 1 (TEF-1) activity from the solution structure of the TEA domain. Proc Natl Acad Sci USA. 2006; 103:17225–17230. DOI: 10.1073/pnas.0607171103 [PubMed: 17085591]

Aurelio O, Aurelio O, Hall DH, Hobert O. Immunoglobulin-domain proteins required for maintenance of ventral nerve cord organization. Science. 2002; 295:686–690. DOI: 10.1126/science.1066642 [PubMed: 11809975]

Barry J, Gu Y, Gu C. Polarized targeting of L1-CAM regulates axonal and dendritic bundling in vitro. Eur J Neurosci. 2010; 32:1618–1631. DOI: 10.1111/j.1460-9568.2010.07447.x [PubMed: 20964729]

Brenner S. The genetics of Caenorhabditis elegans. Genetics. 1974; 77:71–94. [PubMed: 4366476]

Bruce FM, Brown S, Smith JN, Fuerst PG, Erskine L. DSCAM promotes axon fasciculation and growth in the developing optic pathway. Proceedings of the National Academy of Sciences. 2017; 114:1702–1707. DOI: 10.1073/pnas.1618606114

Chatzigeorgiou M, Yoo S, Watson JD, Lee WH, Spencer WC, Kindt KS, Hwang SW, Miller DM III, Treinin M, Driscoll M, Schafer WR. Specific roles for DEG/ENaC and TRP channels in touch and thermosensation in C. elegans nociceptors. Nat Neurosci. 2010; 13:861–868. DOI: 10.1038/nn.2581 [PubMed: 20512132]

Desai C, Garriga G, McIntire SL, Horvitz HR. A genetic pathway for the development of the Caenorhabditis elegans HSN motor neurons. Nature. 1988; 336:638–646. DOI: 10.1038/336638a0 [PubMed: 3200316]

Díaz-Balzac CA, Rahman M, Lazaro-Pena MI, Martin Hernandez LA, Salzberg Y, Aguirre-Chen C, Kaprielian Z, Bülow HE. Muscle- and Skin-Derived Cues Jointly Orchestrate Patterning of Somatosensory Dendrites. Curr Biol. 2016; 26:2379–2387. DOI: 10.1016/j.cub.2016.07.008 [PubMed: 27451901]

Dong X, Liu OW, Howell AS, Shen K. An Extracellular Adhesion Molecule Complex Patterns Dendritic Branching and Morphogenesis. Cell. 2013; 155:296–307. DOI: 10.1016/j.cell.2013.08.059 [PubMed: 24120131]

Feng G, Yi P, Yang Y, Chai Y, Tian D, Zhu Z, Liu J, Zhou F, Cheng Z, Wang X, Li W, Ou G. Developmental stage-dependent transcriptional regulatory pathways control neuroblast lineage progression. Development. 2013; 140:3838–3847. DOI: 10.1242/dev.098723 [PubMed: 23946438]

Grueber WB, Jan LY, Jan YN. Different levels of the homeodomain protein cut regulate distinct dendrite branching patterns of Drosophila multidendritic neurons. Cell. 2003; 112:805–818. [PubMed: 12654247]

Hall DH, Treinin M. How does morphology relate to function in sensory arbors? Trends in Neurosciences. 2011; 34:443–451. DOI: 10.1016/j.tins.2011.07.004 [PubMed: 21840610]

Hunter CS, Rhodes SJ. LIM-homeodomain genes in mammalian development and human disease. Mol Biol Rep. 2005; 32:67–77. DOI: 10.1007/s11033-004-7657-z [PubMed: 16022279]

Jinushi-Nakao S, Arvind R, Amikura R, Kinameri E, Liu AW, Moore AW. Knot/Collier and cut control different aspects of dendrite cytoskeleton and synergize to define final arbor shape. Neuron. 2007; 56:963–978. DOI: 10.1016/j.neuron.2007.10.031 [PubMed: 18093520]

Li W, Kang L, Piggott BJ, Feng Z, Xu XZS. The neural circuits and sensory channels mediating harsh touch sensation in Caenorhabditis elegans. Nature Communications. 2011; 2:315–319. DOI: 10.1038/ncomms1308

Liang X, Dong X, Moerman DG, Shen K, Wang X. Sarcomeres Pattern Proprioceptive Sensory Dendritic Endings through UNC-52/Perlecan in C. elegans. Developmental Cell. 2015; 33:388–400. DOI: 10.1016/j.devcel.2015.03.010 [PubMed: 25982673]

Mohammadi A, Rodgers JB, Kotera I, Ryu WS. Behavioral response of Caenorhabditis elegans to localized thermal stimuli. BMC Neurosci. 2013; 14:1–1. DOI: 10.1186/1471-2202-14-66 [PubMed: 23280045]

Moore AW, Jan LY, Jan YN. hamlet, a binary genetic switch between single- and multiple- dendrite neuron morphology. Science. 2002; 297:1355–1358. DOI: 10.1126/science.1072387 [PubMed: 12193790]

Oren-Suissa M, Hall DH, Treinin M, Shemer G, Podbilewicz B. The fusogen EFF-1 controls sculpting of mechanosensory dendrites. Science. 2010; 328:1285–1288. DOI: 10.1126/science.1189095 [PubMed: 20448153]

O'Brien B, Miller DM III, Miller DM III. Neurodevelopment: Three's a Crowd, Four Is a Receptor Complex. Curr Biol. 2016; 26:R799–801. DOI: 10.1016/j.cub.2016.07.055 [PubMed: 27623260]

Parrish JZ, Kim MD, Jan LY, Jan YN. Genome-wide analyses identify transcription factors required for proper morphogenesis of Drosophila sensory neuron dendrites. Genes & Development. 2006; 20:820–835. DOI: 10.1101/gad.1391006 [PubMed: 16547170]

Rojo Romanos T, Petersen JG, Riveiro AR, Pocock R. A novel role for the zinc-finger transcription factor EGL-46 in the differentiation of gas-sensing neurons in Caenorhabditis elegans. Genetics. 2015; 199:157–163. DOI: 10.1534/genetics.114.172049 [PubMed: 25395666]

Rosenbaum JN, Duggan A, García-Añoveros J. Insm1 promotes the transition of olfactory progenitors from apical and proliferative to basal, terminally dividing and neuronogenic. Neural Dev. 2011; 6:6.doi: 10.1186/1749-8104-6-6 [PubMed: 21284846]

Salzberg Y, Díaz-Balzac CA, Ramirez-Suarez NJ, Attreed M, Tecle E, Desbois M, Kaprielian Z, Bülow HE. Skin-Derived Cues Control Arborization of Sensory Dendritesin Caenorhabditis elegans. Cell. 2013; 155:308–320. DOI: 10.1016/j.cell.2013.08.058 [PubMed: 24120132]

Smith CJ, O'Brien T, Chatzigeorgiou M, Spencer WC, Feingold-Link E, Husson SJ, Hori S, Mitani S, Gottschalk A, Schafer WR, Miller DM III. Sensory Neuron Fates Are Distinguished by a Transcriptional Switch that Regulates Dendrite Branch Stabilization. Neuron. 2013; 79:266–280. DOI: 10.1016/j.neuron.2013.05.009 [PubMed: 23889932]

Smith CJ, Watson JD, Spencer WC, O'Brien T, Cha B, Albeg A, Treinin M, Miller DM III. Time-lapse imaging and cell-specific expression profiling reveal dynamic branching and molecular determinants of a multi-dendritic nociceptor in C. elegans. Developmental Biology. 2010; 345:18–33. DOI: 10.1016/j.ydbio.2010.05.502 [PubMed: 20537990]

Smith CJ, Watson JD, Vanhoven MK, Colón-Ramos DA, Miller DM III. Netrin (UNC-6) mediates dendritic self-avoidance. Nat Neurosci. 2012; 15:731–737. DOI: 10.1038/nn.3065 [PubMed: 22426253]

Tsalik EL, Niacaris T, Wenick AS, Pau K, Avery L, Hobert O. LIM homeobox gene-dependent expression of biogenic amine receptors in restricted regions of the C. elegans nervous system. Developmental Biology. 2003; 263:81–102. [PubMed: 14568548]

Van Vactor D. Adhesion and signaling in axonal fasciculation. Current Opinion in Neurobiology. 1998; 8:80–86. [PubMed: 9568395]

Way JC, Chalfie M. The mec-3 gene of Caenorhabditis elegans requires its own product for maintained expression and is expressed in three neuronal cell types. Genes & Development. 1989; 3:1823–1833. [PubMed: 2576011]

White JG, Southgate E, Thomson JN, Brenner S. The structure of the nervous system of the nematode Caenorhabditis elegans. 1986; 314:1–340.

Wu J, Duggan A, Chalfie M. Inhibition of touch cell fate by egl-44 and egl-46 in C. elegans. Genes & Development. 2001; 15:789–802. DOI: 10.1101/gad.857401 [PubMed: 11274062]

Yu H, Pretot RF, Bürglin TR, Sternberg PW. Distinct roles of transcription factors EGL-46 and DAF-19 in specifying the functionality of a polycystin-expressing sensory neuron necessary for C. elegans male vulva location behavior. Development. 2003; 130:5217–5227. DOI: 10.1242/dev.00678 [PubMed: 12954713]

Zou W, Shen A, Dong X, Tugizova M, Xiang YK, Shen K. A multi-protein receptor-ligand complex underlies combinatorial dendrite guidance choices in C. elegans. eLife. 2016; 5:e18345.doi: 10.7554/eLife.18345 [PubMed: 27705746]

Highlights

- The *C. elegans* PVD neuron contains two classes of sister dendrites.
- Commissural but not pioneer dendrites bundle with other neuronal processes.
- Separate transcriptional pathways specify each type of sister PVD dendrite.
- The Zn finger transcription factor EGL-46 defines commissural dendrites.
- The LIM homeodomain transcription factor MEC-3 regulates both pathways.

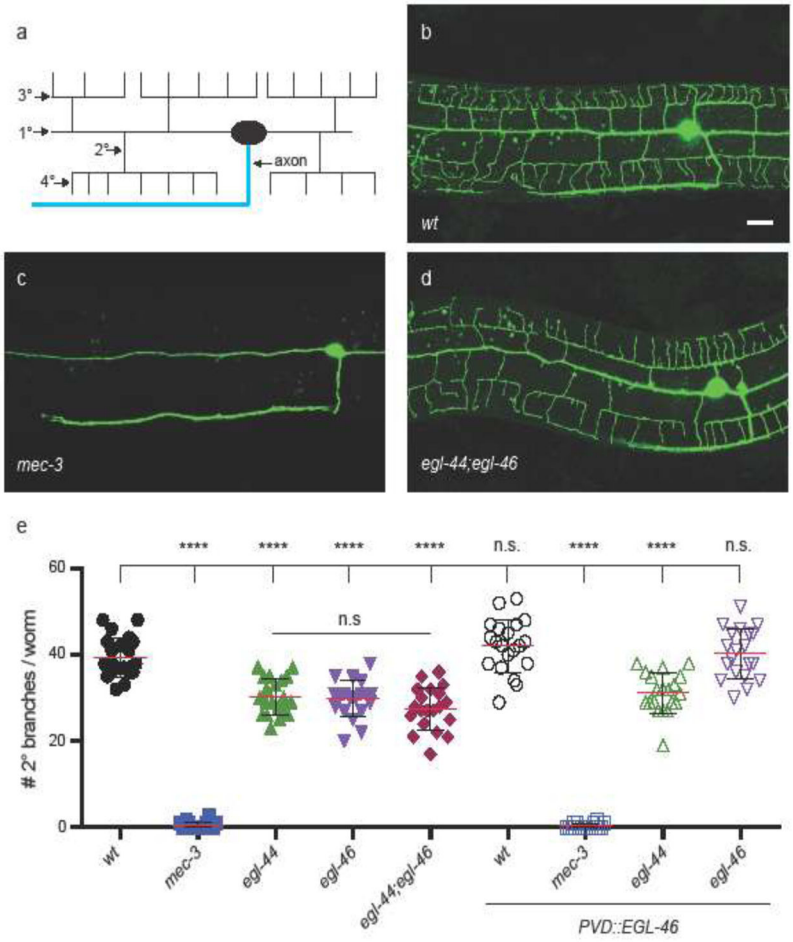

Figure 1. EGL-46 acts cell-autonomously with EGL-44 to promote 2° branches in PVD neurons

(a) Schematic of PVD morphology, highlighting 1°, 2°, 3°, and 4° dendritic branches and single axon; (b–d) confocal images of PVD in wild-type (*wt*) (b) and mutants of *mec-3* (c) and *egl-44;egl-46* (d), visualized with cytosolic GFP driven by the *F49H12.4* promoter; (e) quantification of 2° branches in different genetic backgrounds. Note that PVD expression of EGL-46 with the *F49H12.4* promoter (PVD::EGL-46) restores 2° branches to *egl-46* mutants. Left is anterior, up is dorsal, scale bar = 10 μm, **** indicates $p<0.0001$, n.s. = not significant, one-way ANOVA with Tukey's test for multiple comparisons, error bars represent SEM, $n\geq18$

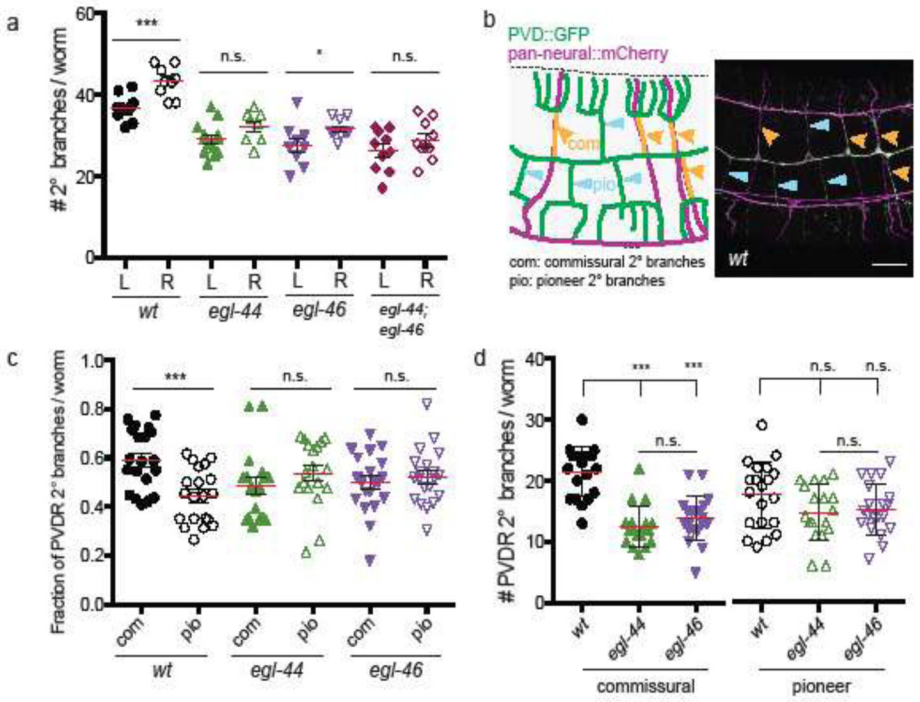

Figure 2. EGL-44 and EGL-46 promote commissural branching

(a) Number of 2° branches for PVDR on the right side (R) vs PVDL on the left (L) (data from Figure 1), n≥8; (b) (left panel) schematic of commissural (com) and pioneer (pio) 2° branches, (right panel) image of PVD::GFP (green) with pan-neural::mCherry (magenta) showing PVDR commissural 2° branches that fasciculate with motor neuron commissures (orange arrow-heads) and pioneer 2° branches that do not fasciculate with motor neuron commissures (blue arrow-heads); (c) fraction of commissural (com) and pioneer (pio) 2° branches for PVDR in different genetic backgrounds; (d) number of commissural and pioneer 2° branches for PVDR in different genetic backgrounds. Left is anterior, up is dorsal, scale bar = 10 μm, * $p<0.05$, *** $p<0.001$, n.s. = not significant, unpaired t-test (a and c), one-way ANOVA with Tukey's test for multiple comparisons (d), error bars represent SEM, n≥18

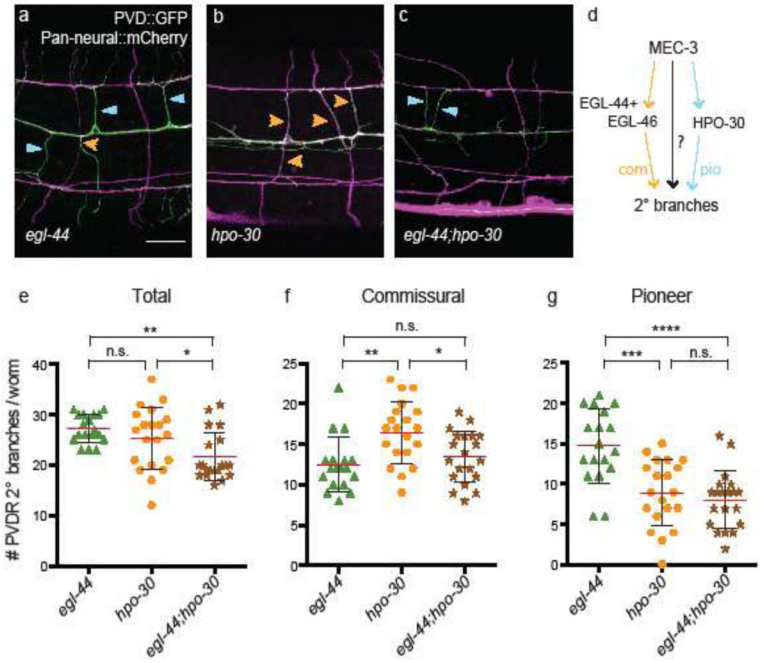

Figure 3. EGL-44 and HPO-30 act in complementary pathways to mediate 2° branch outgrowth

(a–c) confocal images of *egl-44* (a), *hpo-30* (b), and *egl-44;hpo-30* (c) mutants, PVDR labeled with *ser2prom3::GFP* (green) and motor neuron commissures marked with *Prab-3::mCherry* (magenta), commissural (orange arrowheads) vs pioneer (blue arrow heads) 2° branches; (d) proposed genetic pathways for MEC-3-dependent outgrowth of commissural (com) and pioneer (pio) 2° branches; (e–g) quantification of total (e), commissural (f), and pioneer (g) 2° branches in PVDR for *egl-44* and *hpo-30* single mutants and for *egl-44;hpo-30* double mutant animals. Left is anterior, up is dorsal, scale bar = 10 μm, * indicates $p<0.05$, ** indicates $p<0.01$, *** indicates $p<0.001$, **** indicates $p<0.0001$, n.s. = not significant, one-way ANOVA with Tukey's test for multiple comparisons, error bars represent SEM, $n\geq18$. Data for *egl-44* single mutants are the same as in Figure 2.

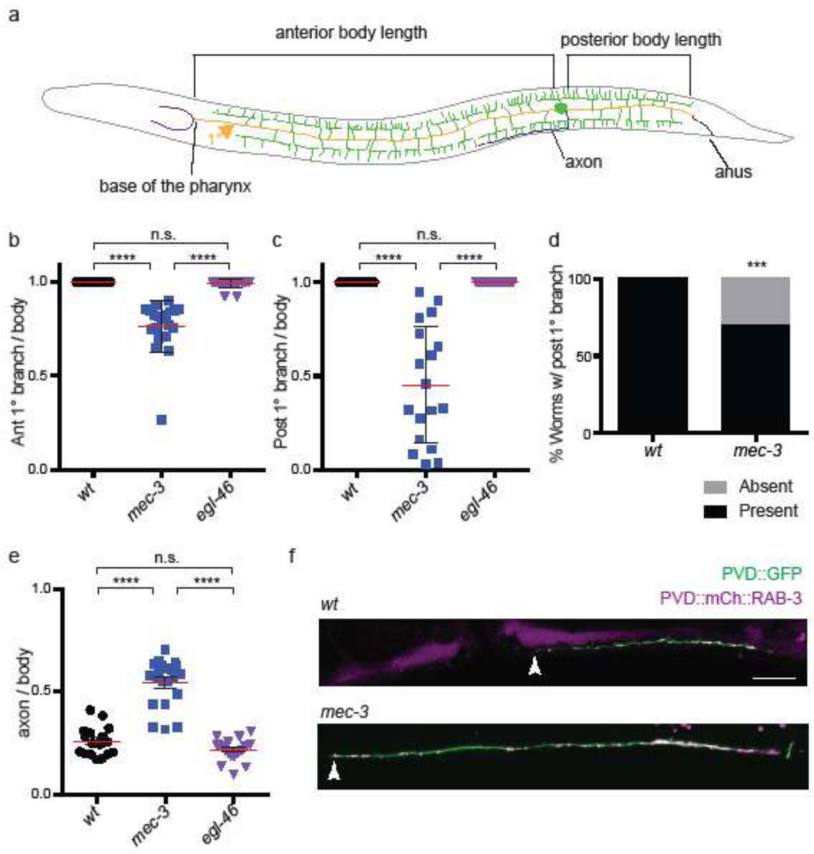

Figure 4. MEC-3, but not EGL-46, regulates 1° branch and axon length

(a) Schematic showing anterior and posterior 1° branches (gold) and body regions relative to the location of the PVD cell body; (b) Ratio of anterior 1° branch length to anterior body; (c) ratio of posterior 1° branch length to posterior body; (d) percentage of worms with (black) or without (gray) the posterior 1° process; (e) ratio of axon length to anterior body; (f) images of the PVD (green) with mCherry-tagged RAB-3 (magenta), white arrows denote RAB-3 puncta localized to the tip of the axon. PVD 1° branches and axon were labeled with cytosolic GFP by *PVD::*GFP integrated strains *wdIs51* (b–d, f bottom) and *wdIs52* (e and f top). *** indicates $p<0.001$, **** indicates $p<0.0001$, n.s. = not significant, Fisher's exact test (d), one-way ANOVA with Tukey's test for multiple comparisons (b, c, and e), error bars represent SEM, $n\geq17$

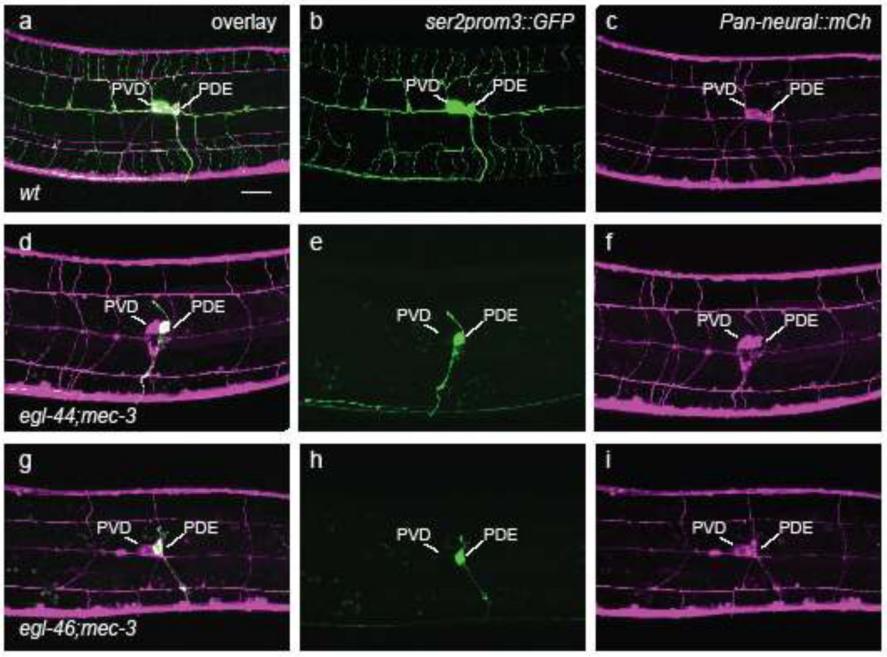

Figure 5. *mec-3* and *egl-46* share redundant roles in regulating PVD genes

Confocal images of PVD marked with *ser2prom3::GFP* (b, e, h), or the pan-neural promoter *Prab-3::mCherry* (c, f, i), or both (a, d, g) in wild type (a–c) and double mutants of *egl-44;mec-3* (d–f) and *egl-46;mec-3* (g–i). Images are maximum-projections. Left is anterior, up is dorsal, scale bar = 10 μm.

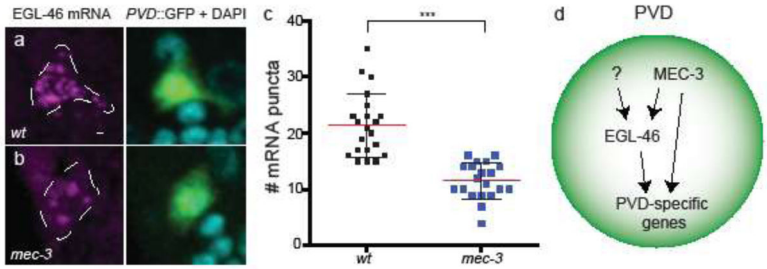

Figure 6. MEC-3 promotes EGL-46 expression

(a–b) Confocal images of *egl-46* smFISH labeling (magenta) in PVD, marked with cytosolic PVD::GFP (green) and DAPI (blue) in (a) *wt* (wild type) and (b) *mec-3*. (c) Quantification of smFISH puncta in *wt* and *mec-3*. (d) Schematic showing gene regulatory cascade involving MEC-3 and EGL-46 in PVD. Left is anterior, up is dorsal, scale bar = 1 μm, *** indicates p<001, Mann-Whitney test, error bars represent SD, n>20.